Phenanthroimidazole-based Covalent Organic Frameworks with Enhanced Activity for the Photocatalytic Hydrogen Evolution Reaction

Cong-Xue Liu,[†] Dong-Lai Pan,[‡] Younggyu Seo,[†] Seungjae Park,[†] Jing-Lan Kan,[‖] Wonyong Choi,[‡] Eunsung Lee*[†]

[†] Department of Chemistry, Pohang University of Science and Technology, Pohang, 37673, Republic of Korea

[‡] Division of Environmental Science and Engineering, Pohang University of Science and Technology, Pohang, 37673, Republic of Korea

[‖] College of Chemistry, Chemical Engineering and Materials Science, Collaborative Innovation Center of Functionalized Probes for Chemical Imaging in Universities of Shandong, Key Laboratory of Molecular and Nano Probes, Ministry of Education, Shandong Normal University, Jinan 250014, P. R. China

ABSTRACT: The rational design of organic semiconductors based on crystalline covalent organic frameworks (COFs) as efficient photocatalysts is highly desirable. In this study, the first example of phenanthroimidazole-based COFs is reported: **PIm-COF1** with an imine linkage and **PIm-COF2** with a β-ketoenamine-linkage. Both COF materials showed substantial optical properties. The average hydrogen evolution rate was 7417.5 $\mu molg^{-1}h^{-1}$ for **PIm-COF2**, which was 20 times higher than that of **PIm-COF1** (358.5 $\mu molg^{-1}h^{-1}$). This can be attributed to the strong donor-acceptor effect of **PIm-COF2** and the continuous separation and transfer of the photoexcited electron-hole pair from the phenanthro[9,10-d]imidazole moiety.

KEYWORDS covalent-organic frameworks, photocatalytic hydrogen evolution, phenanthro[9,10-d]imidazole derivatives
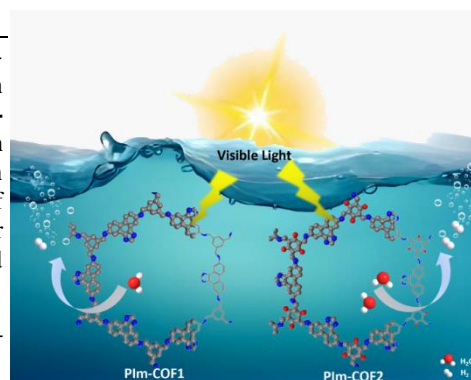
INTRODUCTION

Covalent organic frameworks (COFs) are an emerging class of organic semiconductor materials composed of atomically organized organic subunits connected by strong covalent bonds. The photocatalytic potential of COFs has already been reported.[1,2] The highly crystalline nature of COFs and long-range order in the material not only benefits the light-harvesting capacity and transfer of photogenerated electrons to the surface but also prevents electron-hole pair combination.[3,4] The tunability of building blocks allows for linkage diversity in COFs, such as the β-ketoenamine linkage,[5,6] triazine linkage,[7,8] and olefin linkage,[9,10] which also contributes to the development of COF organic semiconductors with excellent optical and electronic properties. COFs have exhibited a high performance as heterogeneous organic photocatalysts, owing to their high porosity as well as good chemical and thermal stability.[11-13] Three key factors are required for COFs to qualify as photocatalysts; (i) a broad light absorption range, (ii) the separation and migration of photoexcited electron-hole pairs, and (iii) an appropriate oxidation-reduction potential.[14-16] Among them, the generation and migration rate of photogenerated electron-hole pairs determines the progress of the photocatalytic reaction. Therefore, it is essential to rationally design and synthesize COFs with a high capacity for photogenerated electron-hole separation and migration for application in photocatalysis.

Phenanthroimidazole derivatives exhibit a rigid-planar-conjugate structure and ambipolar characteristics owing to the bonding structures of the two nitrogen atoms of the imidazole ring.[17, 18] These derivatives have been widely employed as blue light-emitting materials based on their high carrier mobilities and conductivities, high triplet energies, and high fluorescent efficiencies.[19-21] Therefore, the phenanthroimidazole unit is a good candidate for the fabrication of COFs. However, no well-defined COF synthetic route from phenanthroimidazole derivaties has been reported to date. Herein, we report the first example of phenanthroimidazole-based COFs applied as highly efficient photocatalysts in the hydrogen evolution reaction (HER). Phenanthro[9,10-d]imidazole-5,10-diamine was synthesized as a new building block and was subjected to condensation with 1,3,5-benzenetricarboxaldehyde and 2,4,6-triformylphloroglucinol to yield **PIm-COF1** and **PIm-COF2**, respectively, as potential photocatalysts.

RESULTS AND DISCUSSION

PIm-COF1 and **PIm-COF2** were synthesized via the condensation of 1H-phenanthro[9,10-d] imidazole-5,10-diamine (PIDA, 1) with different aldehyde building blocks, such as 1,3,5-benzenetricarboxaldehyde (BTA, 2) and 2,4,6-triformylphloroglucinol (TP, 3), under solvothermal conditions (Figure 1a and Scheme S1 ESI†). PXRD measurements were performed for all samples to verify the successful formation of **PIm-COF1** and **PIm-COF2**. As shown in Figure 1b, **PIm-COFs** exhibit a typical two-dimensional (2D) layered hexagonal network structure. The PXRD patterns of **PIm-COF1** exhibited an intense peak at 3.5° and three minor peaks at 6.9, 9.0, and 25.5°, which correspond to the (100), (200), (210), and (001)
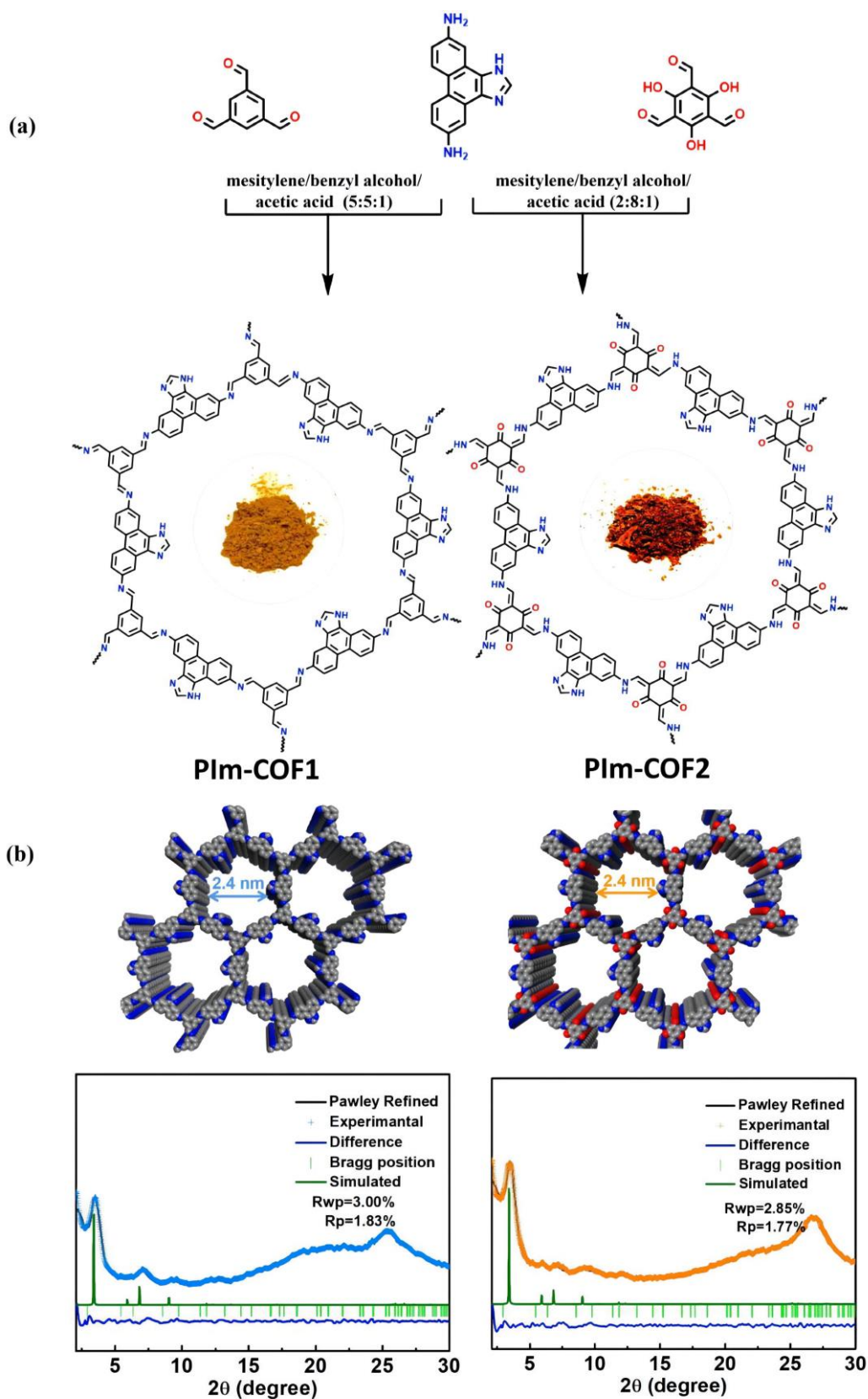
Figure 1. (a) Schematic illustration for the synthesis of **PIm-COFs**. (b) Experimental, Pawley-refined, and AA model simulated powder X-ray diffraction (PXRD) patterns of **PIm-COF1** (right) and **PIm-COF2** (left) (with side views of the ideal eclipsed structures).

reflections, respectively. The PXRD pattern of **PIm-COF2** showed a major diffraction peak at 3.4° and three minor peaks at 5.9, 6.9, 9.0, and 26.0°, which correspond to the (100), (110) (200), (210), and (001) reflections, respectively. The experimental PXRD patterns corresponded well with the patterns simulated using the eclipsed AA layer stacking model (Figure 1b;

Figure S1). The lattice parameters of **PIm-COFs** were extracted using Pawley refinement with the P3 hexagonal space group, and low residual values and acceptable profile differences were observed (Figure 1b; Table S1 and S2).
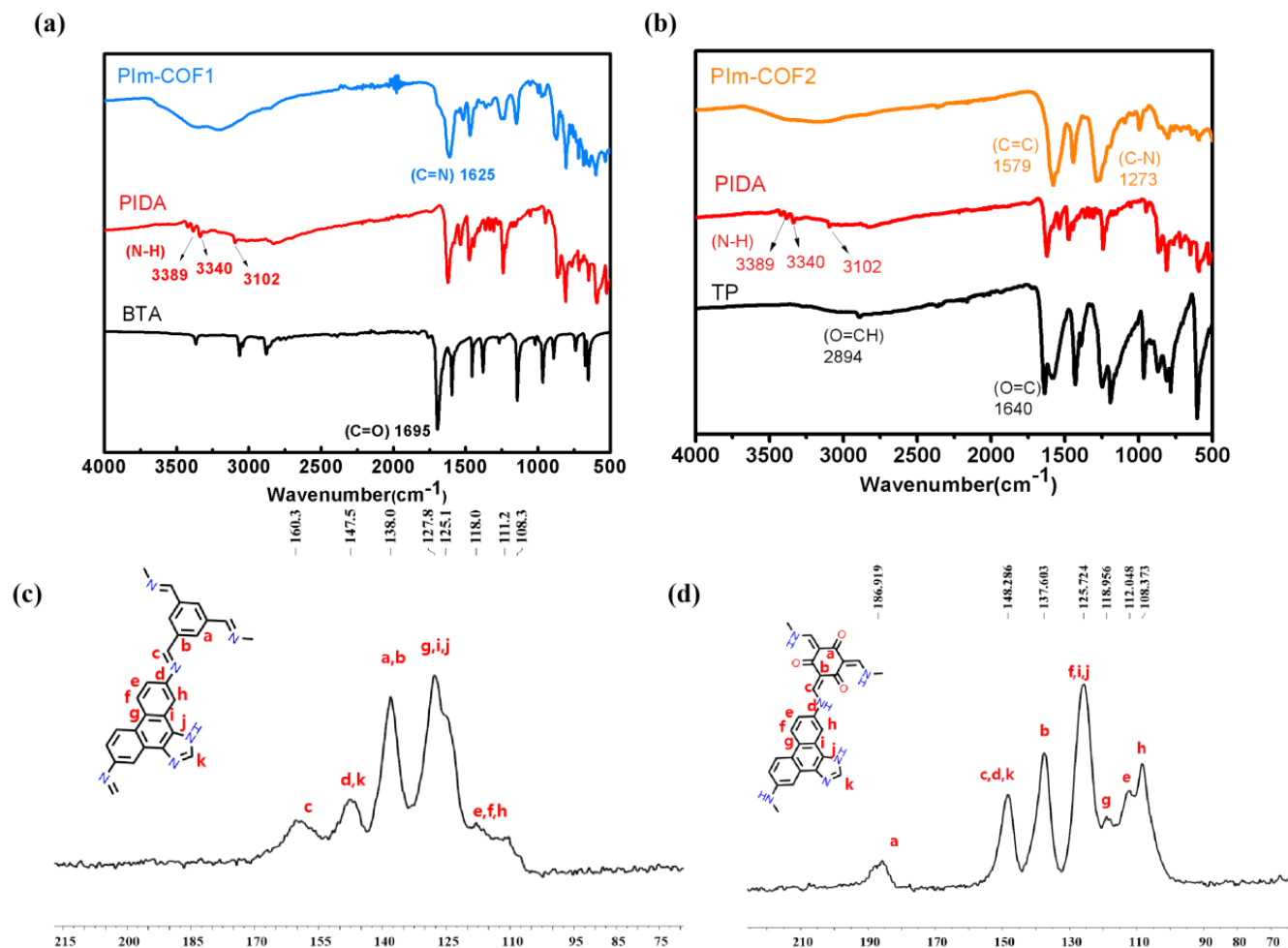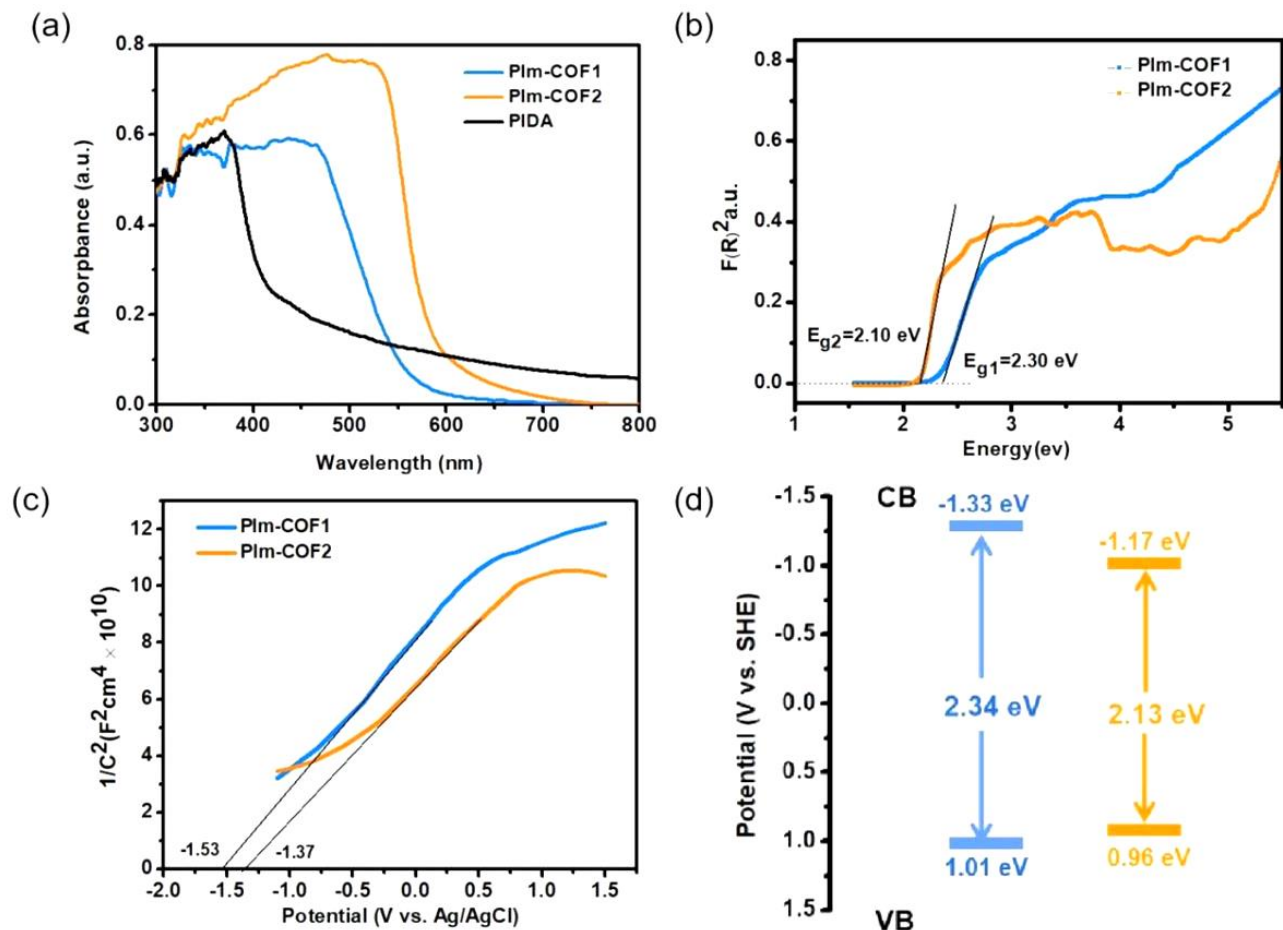

Figure 2. FT-IR spectra of (a) **PIm-COF1** and (b) **PIm-COF2**, and ^{13}C CP/MAS NMR spectra of (c) **PIm-COF1** and (d) **PIm-COF2**.

Fourier transform infrared (FT-IR) and ^{13}C cross-polarization magic angle spinning (CP-MAS) nuclear magnetic resonance (NMR) spectroscopies were performed to examine the chemical composition of **PIm-COF1** and **PIm-COF2** (as shown in Figure 2). The FT-IR spectra of the two samples indicated the complete conversion of the starting materials based on the disappearance of the N−H stretching vibrational peaks of PIDA (3102, 3340, and 3389 cm^{-1}). The disappearance of the C=O stretching vibrational peak of BTA (1695 cm^{-1}) and the appearance of the C=N stretching vibration for **PIm-COF1** (Figure 2a) at 1625 cm^{-1} confirmed the formation of the imine linkage. The characteristic vibration of the C=O stretching band of TP (1640 cm$^{−1}$) disappeared and a strong peak at 1579 cm^{-1} was observed for **PIm-COF2** (Figure 2b), which may be attributed to the C=C stretching vibration of the keto form. Additionally, the absence of hydroxyl (-OH) and imine (C=N) stretching peaks confirmed the existence of the keto form instead of the enol form. Solid-state ^{13}C NMR spectroscopy also confirms that the condensation reaction occurred to form the **PIm-COF1** structure (Figure

2c), as the spectrum exhibits a characteristic peak at 160.3 ppm, which corresponds to the carbon atom of the C=N bond. A signal at 186.9 ppm was observed for the **PIm-COF2** structure, which may be attributed to the carbonyl carbon (C=O) of the keto form (Figure 2d). The FT-IR and XRD results, therefore, confirmed that **PIm-COF1** and **PIm-COF2** formation was successfully achieved.

N_2 adsorption−desorption measurements at 77 K were performed to elucidate the porosity of **PIm-COFs** (Figure S2a). Both **PIm-COF1** and **PIm-COF2** displayed a type-I isotherm, which indicates that the COF materials possess a microporous structure. The Brunauer–Emmett–Teller (BET) surface area was 1004 and 950 m^{2}g^{-1} for **PIm-COF1** and **PIm-COF2**, respectively. **PIm-COFs** had a relatively uniform pore size distribution with an average pore size of 2.2 nm according to the nonlocal density functional theory (DFT) calculation method (Figure S2b). Both **PIm-COFs** exhibited good CO_2 uptake behavior in the isothermic adsorption studies performed at 273 K (Figure S2c). However, the CO_2 adsorption capacity of **PIm-**

COF2 was 64 cm³g⁻¹, which was higher than that of **PIm-COF1** (49 cm³g⁻¹). This may be attributed to the strong affinity between the structure after keto-enol tautomerization and CO_2 molecules.[22,23] The thermal stability of **PIm-COFs** was also analyzed by thermogravimetric analysis (TGA), and the **PIm-COFs** were observed to be thermally stable up to 623 K (Figure S3). To evaluate the chemical stability, activated **PIm-COFs** samples were immersed in 0.1 M ascorbic acid, 3 M aqueous HCl, and 3 M NaOH solutions and DMSO at 298 K for one week. Notably, **PIm-COF1** samples exhibited different degrees of loss in crystallinity, whereas **PIm-COF2** retained strong diffraction peaks (that is, crystallinity) (Figure S4).

The optical band gap energy of **PIm-COF1** and **PIm-COF2** were 2.34 and 2.13 eV, respectively, which was obtained from the Tauc function $(\alpha h\nu)^2$ that is related to the incident photon energy, as shown in Figure 3b. Notably, the UV−vis spectra of **PIm-COF1** and **PIm-COF2** occupied a broader region compared with that of the secondary unit PIDA. **PIm-COF2** exhibited a broader light absorption region compared to **PIm-COF1**, which may be ascribed to the enhanced D-A structure with a stronger conjugation effect between the β-ketoenamine linkage and PIDA ligand.[24-26] MS measurements were performed to determine the semiconductor type and flat band positions of **PIm-COFs** (Figure 3c). The positive slopes observed for both **PIm-**

Figure 3. (a) UV−vis DSR spectra of **PIm-COF1** (blue curve), **PIm-COF2** (orange curve), and ligand PIDA (black curve). (b) Tauc plot transformed reflectance spectra. (c) MS plot for **PIm-COF1** (blue curve) and **PIm-COF2** (orange curve). (d) Energy levels of **PIm-COFs**.

The morphology of **PIm-COFs** was analyzed using scanning electron microscopy (SEM), which exhibited the homogeneous rod-like and microsphere-like crystallites of **PIm-COF1** and **PIm-COF2**, respectively. (Figure S5). The uniform texture of **PIm-COFs** was further confirmed by SEM-EDX mapping, which showed a homogeneous distribution of C, N, and O elements in the COF matrix. Moreover, the morphologies of **PIm-COFs** were analyzed by high-resolution transmission electron microscopy (HR-TEM), and the results matched well with the SEM findings (Figure S6).

The optical absorption properties of **PIm-COFs** were measured using Ultraviolet-visible diffuse reflectance (UV−vis DSR) spectroscopy (Figure 3a), which indicated that **PIm-COFs** samples possessed band structures sufficient to absorb visible light.

COF1 and **PIm-COF2** indicated an n-type semiconducting nature. The calculated conduction-band positions were -1.33 and -1.17 eV for **PIm-COF1** and **PIm-COF2**, respectively. Combined with the bandgap determined from UV-vis DSR data, the valence-band position was determined as 1.01 and 0.96 eV for **PIm-COF1** and **PIm-COF2**, respectively (Figure 3d).

The photoelectrochemical properties of the **PIm-COFs** were evaluated by Electrochemical impedance spectroscopy (EIS) and transient photocurrent measurements. From Figure 4a, Nyquist curves show that the semicircular radius of **PIm-COF2** is smaller than that of **PIm-COF1**, indicating that the **PIm-COF2** has a lower charge transfer resistance and more rapid transfer of the photoinduced electrons than those of **PIm-COF1**. This result was further confirmed by the photocurrent measurements (Figure 4b). As expected, the intensity of the transient

photocurrent response of **PIm-COF2** was higher than that of **PIm-COF1**. Moreover, the photoluminescence (PL) spectrum of **PIm-COF2** showed an emission peak at 620 nm with a very low intensity compared to that of **PIm-COF1** observed at 588 nm (Figure 4c).

experiments for up to 28 h under visible-light irradiation. PXRD patterns indicated that **PIm-COF2** maintained its structural integrity even after 7 cycles (Figure 4f and S8).

The excellent photocatalytic activity of **PIm-COF2** may be attributed to (i) high carrier mobilities, conductivities, and visi-
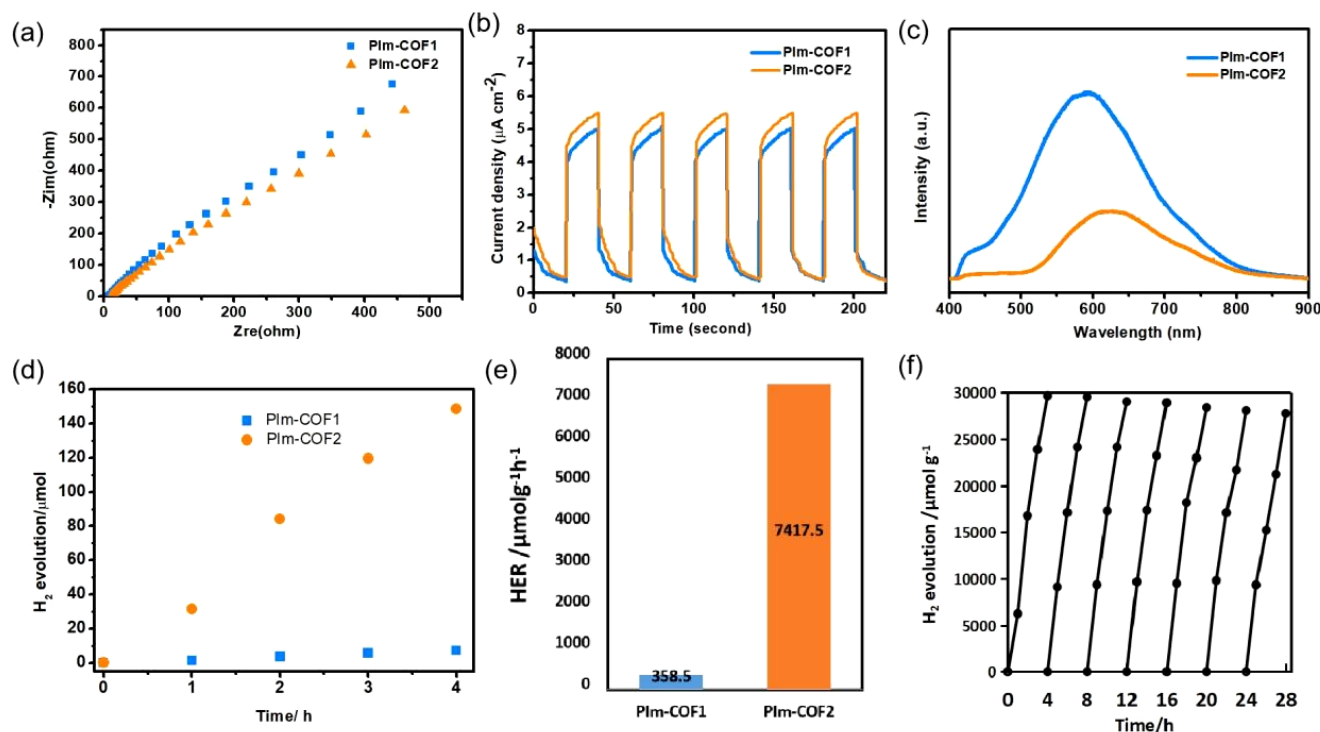
Figure 4.EIS Nyquist plots of **PIm-COF1** (blue curve) and **PIm-COF2** (orange curve); (b) transient photocurrent response of **PIm-COF1** (blue curve) and **PIm-COF2** (orange curve); (c) PL intensity of **PIm-COFs**; (d) H_2 evolution of **PIm-COFs** monitored over 4 h; (e) HER performance of **PIm-COFs**; (f) recyclability experiments of **PIm-COF2**. Conditions: a 5.0 mg sample with 4.4 wt % Pt (from H_2PtCl_6); 0.1 M ascorbic acid in 25.0 mL H_2O; under irradiation of $\lambda \geq 420$ nm.

A broad visible light absorption range, suitable band positions, and a high separation efficiency of electron-hole pairs enable the application of **PIm-COFs** as photocatalysts in the HER. Their photocatalytic HER activity was evaluated in an aqueous solution with the irradiation of visible light ($\lambda \geq 420$ nm). Ascorbic acid was used as a sacrificial agent, and in situ photodeposited Pt nanoparticles (from H_2PtCl_6) served as cocatalysts. The average rate of HER was 7417.5 $\mu molg^{-1}h^{-1}$ for **PIm-COF2**, which was 20 times higher than that of **PIm-COF1** (358.5 $\mu molg^{-1}h^{-1}$) under optimal reaction conditions (Figures 4d, 4e, and S7). The photocatalytic activity of these **PIm-COFs** was also evaluated without the Pt cocatalyst, and **PIm-COF2** was found to retain an HER reactivity of 84.6 $\mu molg^{-1}h^{-1}$ (Figure S7). In the absence of a catalyst in the reaction system, no H_2 was generated. These findings further support the excellent optical properties and photocatalytic activities of newly synthesized β-ketoenamine linked **PIm-COF2**.

The apparent quantum efficiency (AQE) was determined to evaluate the photocatalytic activity of the **PIm-COF** samples (See Supporting Information). Although an AQE of 0.12 % was determined for **PIm-COF1**, the AQE of **PIm-COF2** could reach up to 2.52 %, which is among the highest efficienies reported to date compared to other β-ketoenamine linked COFs used as HER photocatalysts (Table S3). Apart from its excellent photocatalytic performance, **PIm-COF2** exhibited high photocatalytic stability that was determined by performing cycling

ble light adsorption capacity, which were enhanced by the phenanthro[9,10-d]imidazole derivative, (ii) the strong donor-acceptor effect between the 1H-phenanthro[9,10-d] imidazole moiety and keto-form building blocks transformed by enol-keto tautomerism, and (iii) the 2D extended crystalline porous structure with improved light absorption regions, charge transfer, and interactions with aqueous solutions.

CONCLUSION

In summary, a new 1H-phenanthro[9,10-d] imidazole-5,10-diamine derivative was successfully incorporated into a COF framework to form 2D **PIm-COFs**. The H-phenanthro[9,10-d] imidazole moiety imparted **PIm-COFs** with excellent optical properties. Significantly, β-ketoenamine linked **PIm-COF2** showed an enhanced donor-acceptor effect that resulted in a broadened visible light absorption region, a narrowed optical band gap, and an accelerated charge separation and transfer. These properties resulted in a substantial photocatalytic performance between **PIm-COFs** in the HER.

ASSOCIATED CONTENT

Supporting Information
Experimental section, CO_2 adsorption capacity, TGA curves, SEM images, elemental mappings, TEM images, and optimization of the photocatalytic conditions.

AUTHOR INFORMATION

Corresponding Author

eslee@postech.ac.kr

ORCID

Eunsung Lee: 0000-0002-1507-098X

Notes

The authors declare no competing financial interest.

REFERENCES

(1) (a) Wan, S.; Guo, J.; Kim, J.; Ihee, H.; Jiang, D., A belt-shaped, blue luminescent, and semiconducting covalent organic framework. *Angew. Chem., Int. Ed.* **2008**, *47*, 8826-8830. (b) Joshi, T.; Chen, C.; Li, H.; Diercks, C. S.; Wang, G.; Waller, P. J.; Li, H.; Bredas, J. L.; Yaghi, O. M.; Crommie, M. F., Local Electronic Structure of Molecular Heterojunctions in a Single-Layer 2D Covalent Organic Framework. *Adv. Mater.* **2019**, *31*, 1805941. (c) Geng, K.; He, T.; Liu, R.; Dalapati, S.; Tan, K. T.; Li, Z.; Tao, S.; Gong, Y.; Jiang, Q.; Jiang, D., Covalent Organic Frameworks: Design, Synthesis, and Functions. *Chem. Rev.* **2020**, *120*, 8814-8933. (d) Leith, G. A.; Martin, C. R.; Mayers, J. M.; Kittikhunnatham, P.; Larsen, R. W.; Shustova, N. B., Confinement-guided photophysics in MOFs, COFs, and cages. *Chem. Soc. Rev.* **2021**, *50*, 4382-4410.

(2) (a) Ding, S. Y.; Wang, W., Covalent organic frameworks (COFs): from design to applications. *Chem. Soc. Rev.* **2013**, *42*, 548-568. (b) Li, Y.; Guo, L.; Lv, Y.; Zhao, Z.; Ma, Y.; Chen, W.; Xing, G.; Jiang, D.; Chen, L., Polymorphism of 2D Imine Covalent Organic Frameworks. *Angew. Chem., Int. Ed.* **2021**, *60*, 5363-5369. (c) Jin, E.; Li, J.; Geng, K.; Jiang, Q.; Xu, H.; Xu, Q.; Jiang, D., Designed synthesis of stable light-emitting two-dimensional sp2 carbon-conjugated covalent organic frameworks. *Nat. Commun.* **2018**, *9*, 4143. (d) Wang, G. B.; Zhu, F. C.; Lin, Q. Q.; Kan, J. L.; Xie, K. H.; Li, S.; Geng, Y.; Dong, Y. B., Rational design of benzodifuran-functionalized donor-acceptor covalent organic frameworks for photocatalytic hydrogen evolution from water. *Chem. Commun.* **2021**, *57*, 4464-4467.

(3) (a) Chen, X.; Geng, K.; Liu, R.; Tan, K. T.; Gong, Y.; Li, Z.; Tao, S.; Jiang, Q.; Jiang, D., Covalent Organic Frameworks: Chemical Approaches to Designer Structures and Built-In Functions. *Angew. Chem., Int. Ed.* **2020**, *59*, 5050-5091. (b) Wang, G.-B.; Li, S.; Yan, C.-X.; Zhu, F.-C.; Lin, Q.-Q.; Xie, K.-H.; Geng, Y.; Dong, Y.-B., Covalent organic frameworks: emerging high-performance platforms for efficient photocatalytic applications. *J. Mater. Chem. A.* **2020**, *8*, 6957-6983. (c) Thomas, S.; Li, H.; Dasari, R. R.; Evans, A. M.; Castano, I.; Allen, T. G.; Reid, O. G.; Rumbles, G.; Dichtel, W. R.; Gianneschi, N. C.; Marder, S. R.; Coropceanu, V.; Brédas, J.-L., Design and synthesis of two-dimensional covalent organic frameworks with four-arm cores: prediction of remarkable ambipolar charge-transport properties. *Mater. Horizons.* **2019**, *6*, 1868-1876. (d) Wei, P. F.; Qi, M. Z.; Wang, Z. P.; Ding, S. Y.; Yu, W.; Liu, Q.; Wang, L. K.; Wang, H. Z.; An, W. K.; Wang, W., Benzoxazole-Linked Ultrastable Covalent Organic Frameworks for Photocatalysis. *J. Am. Chem. Soc.* **2018**, *140*, 4623-4631.

(4) (a) Keller, N.; Bein, T., Optoelectronic processes in covalent organic frameworks. *Chem. Soc. Rev.* **2021**, *50*. 1813-1845. (b) He, T.; Geng, K.; Jiang, D., Engineering Covalent Organic Frameworks for Light-Driven Hydrogen Production from Water. *ACS Mater. Lett.* **2019**, *1*, 203-208.

(5) DeBlase, C. R.; Silberstein, K. E.; Truong, T. T.; Abruna, H. D.; Dichtel, W. R., beta-Ketoenamine-linked covalent organic frameworks capable of pseudocapacitive energy storage. *J. Am. Chem. Soc.* **2013**, *135*, 16821-16824.

(6) Pachfule, P.; Acharjya, A.; Roeser, J.; Langenhahn, T.; Schwarze, M.; Schomacker, R.; Thomas, A.; Schmidt, J., Diacetylene Functionalized Covalent Organic Framework (COF) for Photocatalytic Hydrogen Generation. *J. Am. Chem. Soc.* **2018**, *140*, 1423-1427.

(7) (a) Kuhn, P.; Antonietti, M.; Thomas, A., Porous, covalent triazine-based frameworks prepared by ionothermal synthesis. *Angew. Chem., Int. Ed.* **2008**, *47*, 3450-3453. (b) Dai, C.; He, T.; Zhong, L.; Liu, X.; Zhen, W.; Xue, C.; Li, S.; Jiang, D.; Liu, B., 2,4,6-Triphenyl-1,3,5-Triazine Based Covalent Organic Frameworks for Photoelectrochemical H_2 Evolution. *Adv. Mater. Interfaces.* **2021**, *8*, 2002191. (c) Wang, Y.; Hao, W.; Liu, H.; Chen, R.; Pan, Q.; Li, Z.; Zhao, Y., Facile construction of fully sp(2)-carbon conjugated two-dimensional covalent organic frameworks containing benzobisthiazole units. *Nat. Commun.* **2022**, *13*, 100.

(8) (a) Kewei Wang, L.-M. Y., Xi Wang, Liping Guo, Guang Cheng, Chun Zhang, Shangbin Jin, Bien Tan, and Andrew Cooper, Covalent Triazine Frameworks via a Low-Temperature Polycondensation Approach. *Angew. Chem. Int. Ed.* **2017**, *56*, 14149 –14153. (b) Kulkarni, R.; Noda, Y.; Kumar Barange, D.; Kochergin, Y. S.; Lyu, P.; Balcarova, B.; Nachtigall, P.; Bojdys, M. J., Real-time optical and electronic sensing with a beta-amino enone linked, triazine-containing 2D covalent organic framework. *Nat. Commun.* **2019**, *10*, 3228. (c) Li, Y.; Han, Y.; Chen, M.; Feng, Y.; Zhang, B., Construction of a flexible covalent organic framework based on triazine units with interesting photoluminescent properties for sensitive and selective detection of picric acid. *RSC Adv.* **2019**, *9*, 30937-30942.

(9) (a) Lyu, H.; Diercks, C. S.; Zhu, C.; Yaghi, O. M., Porous Crystalline Olefin-Linked Covalent Organic Frameworks. *J. Am. Chem. Soc.* **2019**, *141*, 6848-6852. (b) Xu, J.; He, Y.; Bi, S.; Wang, M.; Yang, P.; Wu, D.; Wang, J.; Zhang, F., An Olefin-Linked Covalent Organic Framework as a Flexible Thin-Film Electrode for a High-Performance Micro-Supercapacitor. *Angew. Chem. Int. Ed.* **2019**, *58*, 12065-12069.

(10) (a) Wei, S.; Zhang, F.; Zhang, W.; Qiang, P.; Yu, K.; Fu, X.; Wu, D.; Bi, S.; Zhang, F., Semiconducting 2D Triazine-Cored Covalent Organic Frameworks with Unsubstituted Olefin Linkages. *J. Am. Chem. Soc.* **2019**, *141*, 14272-14279. (b) Wang, Z.; Yang, Y.; Zhao, Z.; Zhang, P.; Zhang, Y.; Liu, J.; Ma, S.; Cheng, P.; Chen, Y.; Zhang, Z., Green synthesis of olefin-linked covalent organic frameworks for hydrogen fuel cell applications. *Nat. Commun.* **2021**, *12*, 1982.

(11) (a) Liu, R.; Tan, K. T.; Gong, Y.; Chen, Y.; Li, Z.; Xie, S.; He, T.; Lu, Z.; Yang, H.; Jiang, D., Covalent organic frameworks: an ideal platform for designing ordered materials and advanced applications. *Chem. Soc. Rev.* **2021**, *50*, 120-242. (b) Zhang, F.; Hao, H.; Dong, X.; Li, X.; Lang, X., Olefin-linked covalent organic framework nanotubes based on triazine for selective oxidation of sulfides with O2 powered by blue light. *Appl. Catal. B.* **2022**, *305*, 121027. (c) Evans, A. M.; Ryder, M. R.; Ji, W.; Strauss, M. J.; Corcos, A. R.; Vitaku, E.; Flanders, N. C.; Bisbey, R. P.; Dichtel, W. R., Trends in the thermal stability of two-dimensional covalent organic frameworks. *Faraday Discuss.* **2021**, *225*, 226-240.

(12) Barman, S.; Singh, A.; Rahimi, F. A.; Maji, T. K., Metal-Free Catalysis: A Redox-Active Donor-Acceptor Conjugated Microporous Polymer for Selective Visible-Light-Driven CO_2 Reduction to CH_4. *J. Am. Chem. Soc.* **2021**, *14*, 16284-16292.

(13) Liu, L.; Gao, M. Y.; Yang, H.; Wang, X.; Li, X.; Cooper, A. I., Linear Conjugated Polymers for Solar-Driven Hydrogen Peroxide Production: The Importance of Catalyst Stability. *J. Am. Chem. Soc.* **2021**, *143*, 19287-19293.

(14) (a) Zhang, T.; Xing, G.; Chen, W.; Chen, L., Porous organic polymers: a promising platform for efficient photocatalysis. *Mater. Chem. Front.* **2020**, *4*, 332-353. (b) Wang, H.; Wang, H.; Wang, Z.; Tang, L.; Zeng, G.; Xu, P.; Chen, M.; Xiong, T.; Zhou, C.; Li, X.; Huang, D.; Zhu, Y.; Wang, Z.; Tang, J., Covalent organic framework photocatalysts: structures and applications. *Chem. Soc. Rev.* **2020**, *49*, 4135-4165. (c) Sharma, R. K.; Yadav, P.; Yadav, M.; Gupta, R.; Rana, P.; Srivastava, A.; Zbořil, R.; Varma, R. S.; Antonietti, M.; Gawande,

M. B., Recent development of covalent organic frameworks (COFs): synthesis and catalytic (organic-electro-photo) applications. *Mater. Horizons.* **2020**, *7*, 411-454.

(15) (a) Wang, T.-X.; Liang, H.-P.; Anito, D. A.; Ding, X.; Han, B.-H., Emerging applications of porous organic polymers in visible-light photocatalysis. *J. Mater. Chem. A.* **2020**, *8*, 7003-7034. (b) Zhi, Y.; Wang, Z.; Zhang, H. L.; Zhang, Q., Recent Progress in Metal-Free Covalent Organic Frameworks as Heterogeneous Catalysts. *Small .***2020**, *16*, e2001070.

(16) (a) Hu, X.-L.; Li, H.-G.; Tan, B.-E., COFs-based Porous Materials for Photocatalytic Applications. Chinese J. Polym.Sci. 2020, 38, 673-684. (b) Q, Yang.; Luo, M-L.; Kewei Liu.; H-M, Cao.; H-J, Yan.; Covalent organic frameworks for photocatalytic applications, *Appl. Catal. B.* **2020**, *276*, 119174. (c) Zhao, J.; Ren, J.; Zhang, G.; Zhao, Z.; Liu, S.; Zhang, W.; Chen, L., *Chem. Eur. J.* **2021**, *27*, 10781-10797.

(17) Sonalin, S.; Kurlekar, K.; Anjali, A.; Imran, P. M.; Nagarajan, S., Synthesis of Phenanthro[9,10- d]imidazoles and their Potential Applications in Solution Processable Bottom-Gated OFETs. *Asian J. Org. Chem.* **2020**, *9*, 939-946.

(18) Chen, S.; Wu, Y.; Zhao, Y.; Fang, D., Deep blue organic light-emitting devices enabled by bipolar phenanthro[9,10-d]imidazole derivatives. *RSC Adv.* **2015**, *5*, 72009-72018.

(19) Tagare, J.; Vaidyanathan, S. Recent development of phenanthroimidazole-based fluorophores for blue organic light-emitting diodes (OLEDs): an overview. *J. Mater. Chem. C.* **2018**, *6*, 10138-10173.

(20)Yu, Y.; Zhao, R.; Liu, H.; Zhang, S.; Zhou, C.; Gao, Y.; Li, W.; Yang, B., Highly efficient deep-blue light-emitting material based on V-Shaped donor-acceptor triphenylamine-phenanthro[9,10-d]imidazole molecule. *Dyes. Pigments*. **2020**, *180*, 108511-108518.

(21)Kula, S.; Ledwon, P.; Maroń, A. M.; Siwy, M.; Grzelak, J.; Szalkowski, M.; Maćkowski, S.; Schab-Balcerzak, E., Synthesis, photophysical properties and electroluminescence characterization of 1-phenyl-1H-phenanthro[9,10-d]imidazole derivatives with N-donor substituents. *Dyes. Pigments.* **2021**, *192*, 109437-109446.

(22) Idris, M.; Coburn, C.; Fleetham, T.; Milam-Guerrero, J.; Djurovich, P. I.; Forrest, S. R.; Thompson, M. E., Phenanthro[9,10-d]triazole and imidazole derivatives: high triplet energy host materials for blue phosphorescent organic light emitting devices. *Mater. Horizons.* **2019**, *6*, 1179-1186.

(23) Kaleeswaran, D.; Vishnoi, P.; Murugavel, R., [3+3] Imine and β-ketoenamine tethered fluorescent covalent-organic frameworks for CO2 uptake and nitroaromatic sensing. *J. Mater. Chem. C.* **2015**, *3*, 7159-7171.

(24) El-Mahdy, A. F. M.; Hung, Y.-H.; Mansoure, T. H.; Yu, H.-H.; Hsu, Y.-S.; Wu, K. C. W.; Kuo, S.-W., Synthesis of [3 + 3] β-ketoenamine-tethered covalent organic frameworks (COFs) for high-performance supercapacitance and CO2 storage. *J. Taiwan. Inst. Chem. E.* **2019**, *103*, 199-208.

(25) Peng, L.; Chang, S.; Liu, Z.; Fu, Y.; Ma, R.; Lu, X.; Zhang, F.; Zhu, W.; Kong, L.; Fan, M., Visible-light-driven photocatalytic CO2 reduction over ketoenamine-based covalent organic frameworks: role of the host functional groups. *Catal. Sci. Technol.* **2021**, *11*, 1717-1724.

(26) Daugherty, M. C.; Vitaku, E.; Li, R. L.; Evans, A. M.; Chavez, A. D.; Dichtel, W. R., Improved synthesis of beta-ketoenamine-linked covalent organic frameworks via monomer exchange reactions. *Chem. Commun.* **2019**, *55*, 2680-2683.

(27) Lin, C.; Liu, X.; Yu, B.; Han, C.; Gong, L.; Wang, C.; Gao, Y.; Bian, Y.; Jiang, J., Rational Modification of Two-Dimensional Donor-Acceptor Covalent Organic Frameworks for Enhanced Visible Light Photocatalytic Activity. *ACS Appl. Mater. Inter.* **2021**, *13*, 27041-27048.

.